The 8th European Congress on Computational Methods in Applied Sciences and Engineering
ECCOMAS Congress 2022
5-–9 June 2022, Oslo, Norway

ANALYSIS OF HIGH-ORDER INTERPOLATION SCHEMES FOR SOLVING LINEAR PROBLEMS IN UNSTRUCTURED MESHES USING THE FINITE VOLUME METHOD

Pablo Castrillo[1,3], Eugenio Schillaci[1,2] and Joaquim Rigola[1]

[1]Centre Tecnològic de Transferència de Calor (CTTC)-Universitat Politècnica de Catalunya BARCELONA TECH (UPC), Terrassa, Spain.
pablo.castrillo@upc.edu, joaquim.rigola@upc.edu. URL: www.cttc.upc.edu

[2] Termo Fluids SL, Carrer Magi Colet 8, 08204 Sabadell (Barcelona), Spain.
eugenio@termofluids.com. URL: www.termofluids.com

[3] Instituto de Estructuras y Transporte, Facultad de Ingeniería, Universidad de la República, Montevideo, Uruguay. pabloc@fing.edu.uy. URL: www.fing.edu.uy/es/iet

Key words: Finite Volume Method, High-order Interpolation, Unstructured Meshes, Linear Elasticity.

Abstract. Finite-volume strategies in fluid-structure interaction problems would be of crucial importance in many engineering applications such as in the analysis of reed valves in reciprocating compressors. The efficient implementation of this strategy passes from the formulation of reliable high-order schemes on 3D unstructured meshes. The development of high-order models is essential in bending-dominant problems, where the phenomenon of shear blocking appears. In order to solve this problem, it is possible to either increase the number of elements or increase the interpolation order of the main variable. Increasing the number of elements does not always yield good results and implies a very high computational cost that, in real problems, is inadmissible. Using unstructured meshes is also vital because they are necessary for real problems where the geometries are complex and depart from canonical rectangular or regular shapes. This work presents a series of tests to demonstrate the feasibility of a high-order model using finite volumes for linear elasticity on unstructured and structured meshes. The high-order interpolation will be performed using two different schemes such as the Moving Least Squares (MLS) and the Local Regression Estimators (LRE). The reliability of the method for solving 2D and 3D problems will be verified by solving some known test cases with an analytical solution such as a thin beam or problems where stress concentrations appear.

1 INTRODUCTION

Since its most original formulations, the Finite Volume Method (FVM) is usually associated with fluid and heat transfer problems. One of the main advantages of the FVM consists in its capability to enforce the conservation of quantities at a discretized level (forces between adjacent control volumes are directly balanced). The adoption of FVM strategies for the resolution of governing equations in both solid and fluid would lead to highly efficient couplings in

fluid–structure interaction (FSI) problems. However, the procedures used to solve the solid and fluid problems must be compatible in some aspects such as the structure of the mesh, the method to discretize the equations spatially, and the exchange of information in the fluid-structure interface [1]. As a result, adopting the obtained finite-volume strategy in FSI problems would be of crucial importance in many engineering applications such as the resolution of reed valves in reciprocating compressors. Those strategies currently employ different numerical methods for the resolution of the fluid flow and the solid movement, e.g. in Tofique et al. [2] LES models are used to solve the fluid flow while a 2D mode superposition method together with an impact penalty method is employed to represent the valve. Pressure fields then need to be exported to obtain valve internal stresses using a solid dynamic strategy, e.g. in Castrillo et al. [3] a finite element method together with a dynamic impact modelization is employed.

In [4, 5, 6] high-order interpolation schemes on unstructured meshes are used for problems in fluid mechanics and aeroacoustics. However, a general lack of material regarding high-order finite volume schemes for solid dynamic problems has been highlighted in previous bibliographic studies [7]. Among the works that deserve to be mentioned, [8] proposed a FVM with a high-order interpolation scheme for the main variable in structured two-dimensional Cartesian meshes, while Cardiff et al. [9] proposed a linear interpolation coupled Finite Volume Method for unstructured meshes.

The current work is distributed as follows. Section 2.1 presents the equations that govern the linear elasticity problem. Then, in Section 2.2, the discretization using finite volumes with a high-order interpolation method presented in [10] is highlighted. In Section 3 different tests are performed to demonstrate the extensibility of the model towards the resolution of the reed valve problem mentioned above. The latter is characterized by an unstructured mesh, distributed loads, and three-dimensional geometry.

2 NUMERICAL METHODOLOGY

2.1 Governing equations

In this work, some hypotheses have been considered: (1) Homogeneous and isotropic material; (2) linear elastic material behavior; (3) geometric nonlinearity effects are not considered; and (4) static problem. Taking into account the previous hypotheses, the equilibrium equation is:

$$\nabla \cdot \boldsymbol{\sigma}(\mathbf{x}) + \mathbf{b}(\mathbf{x}) = \mathbf{0} \quad \forall\, \mathbf{x} \in \Omega\,, \tag{1}$$

where Ω is the reference configuration, $\mathbf{b}$ is the body force, and $\boldsymbol{\sigma}$ is the Cauchy stress tensor. Stresses and displacements are related with the constitutive equation:

$$\boldsymbol{\sigma} = \mu\nabla\mathbf{u} + \mu\nabla^{\mathrm{T}}\mathbf{u} + \lambda\,\mathrm{tr}\,(\nabla\mathbf{u})\,\mathbf{I}\,, \tag{2}$$

where $\mathbf{u}$ is the displacement field, μ and λ are the Lamé parameters, and $\mathbf{I}$ is the identity tensor.

2.2 Finite volume discretization

In order to apply the FVM it is necessary to discretize the body Ω in N_v finite volumes (internal volumes and boundary faces) where Eq. 1 has to be satisfied for each one of them.

Integrating Eq. (1) over the finite volume Ω_v and using Gauss's theorem of divergence, it is obtained that:

$$\int_{\partial\Omega_v} \boldsymbol{\sigma}\,\mathbf{n}\,\mathrm{d}A + \int_{\Omega_v} \mathbf{b}\,\mathrm{d}V = \mathbf{0}\,, \tag{3}$$

where $\mathbf{n}$ is the outward unit normal of surface $\partial\Omega_v$. Using numerical quadrature [11, 12], Eq. (3) gives:

$$\sum_{f=1}^{f=N_f}\left[\sum_{g=1}^{g=N_g}\alpha_g\,\boldsymbol{\sigma}(\mathbf{x}_{f,g})\,\mathbf{n}_f\right] + \sum_{m=1}^{m=N_m}\beta_m\,\mathbf{b}\,(\mathbf{x}_m) = \mathbf{0}\,, \tag{4}$$

where N_f is the number of faces of the discretized finite volume Ω_v, N_g is the number of quadrature points used to approximate the integral on the face Σ_f, α_g are the quadrature weights (including Jacobian terms), N_m and β_m are the number of quadrature points and weights to approximate the body force, respectively. Replacing Eq. (2) into Eq. (4):

$$\sum_{f=1}^{f=N_f}\left[\sum_{g=1}^{g=N_g}\alpha_g\left[\mu\nabla\mathbf{u}(\mathbf{x}_{f,g}) + \mu\nabla^{\mathrm{T}}\mathbf{u}(\mathbf{x}_{f,g}) + \lambda\,\mathrm{tr}\left(\nabla\mathbf{u}(\mathbf{x}_{f,g})\right)\mathbf{I}\right]\mathbf{n}_f\right] + \sum_{m=1}^{m=N_m}\beta_m\,\mathbf{b}_m = \mathbf{0}\,. \tag{5}$$

In the next section, the high-order method is presented, where a high-order expression is sought for the $\nabla\mathbf{u}$ as a function of the nodal values of $\mathbf{u}$ (here, nodal values represent the values at the centroids of the finite volumes).

2.2.1 High-order interpolation

For the interpolation, coefficients that allow expressing the displacement field and its derivatives as a function of nodal values are needed:

$$\mathbf{u}(\tilde{\mathbf{x}}) = \sum_{n=1}^{n=N_n} c_n(\tilde{\mathbf{x}})\,\mathbf{u}_n,\ \frac{\partial\mathbf{u}}{\partial x}(\tilde{\mathbf{x}}) = \sum_{n=1}^{n=N_n} c_{x,n}(\tilde{\mathbf{x}})\,\mathbf{u}_n\,, \tag{6}$$

where N_n is the number of surrounding points used for the interpolation [10]. For the derivatives respect to y and z others coefficients, $c_{y,n}$ and $c_{z,n}$ respectively, are obtained. These coefficients are obtained with a high-order interpolation method, making a high-order interpolation of $\mathbf{u}$ and its derivatives (gradient of $\mathbf{u}$). In this work, two methods are used to obtain the coefficients: the Moving Least Squares (MLS) [13] and the Local Regression Estimators (LRE) [14, 15].

MLS and LRE methods minimize a weighted sum of squares to obtain the coefficients c_n for the interpolation of $\mathbf{u}$. This minimization ends in solving a system of equations, which is generally poorly conditioned. The coefficients c_n are the same for both interpolations; the difference lies in the coefficients for the interpolation of the derivatives:

- In MLS it is necessary to solve more systems of badly conditioned equations.
- In LRE the coefficients are obtained from the first system.

A more detailed description of the methods and how to deal with the bad-conditioned systems could be found in [10].

In order to apply the high-order methodology to Eq. 5 it is necessary to obtain the interpolation coefficients for each gauss point of each face of the finite volume discretization, obtaining:

$$\sum_{f=1}^{f=N_f}\left[\sum_{g=1}^{g=N_g}\alpha_g\left(\mu\sum_{n=1}^{n=N_n}\left(\mathbf{c}_{\mathbf{x},n}\cdot\mathbf{n}_f\right)\mathbf{I}\,\mathbf{u}_n+\mu\sum_{n=1}^{n=N_n}\left(\mathbf{c}_{\mathbf{x},n}\mathbf{n}_f^{\mathrm{T}}\right)\mathbf{u}_n+\lambda\sum_{n=1}^{n=N_n}\left(\mathbf{n}_f\,\mathbf{c}_{\mathbf{x},n}^{\mathrm{T}}\right)\mathbf{u}_n\right)\right]+\sum_{m=1}^{m=N_m}\mathbf{b}_m\,\beta_m=\mathbf{0}\,, \quad (7)$$

where $\mathbf{c}_{\mathbf{x},n}^{\mathrm{T}}(\mathbf{x}_{f,g})=[c_{x,n}(\mathbf{x}_{f,g})\ c_{y,n}(\mathbf{x}_{f,g})\ c_{z,n}(\mathbf{x}_{f,g})]$ are the interpolation coefficients of the derivatives. In [10] a detailed description on how to obtain the coefficients is presented, furthermore in [10] it is possible to find out precisely how to incorporate the boundary conditions: Dirichlet, Neumann or Symmetry conditions.

3 NUMERICAL RESULTS

In this section, numerical results obtained with the proposed method are presented. In Section 3.1 two examples for two-dimensional problems are presented; more examples and an extended analysis for two-dimensional problems could be found in [10]. Then, in Section 3.2, examples for three-dimensional problems are presented and analyzed for structured meshes.

In what follows p_i represents the interpolation order, e.g. interpolation p_1 is linear. The software FreeFEM [16] with linear (p_1) or quadratic (p_2) interpolation (FF p_1 and FF p_2 in figures and tables) and the 2nd-order method developed by Cardiff [9] are used to compare with the proposed method.

3.1 Two-dimensional examples

In [17, 18] it is possible to find many examples of linear elasticity with analytical solution, which are generally approximated. The example presented in Section 3.1.1 is a beam under a distributed load, in which case the shear-locking effect appears. Then in Section 3.1.2 it is presented an example where unstructured meshes are needed due to its geometry.

To solve these examples the MLS and LRE methods are used. Four interpolations are used: p_1 (linear), p_2 (quadratic), p_3 (cubic) and p_4 (quartic). The numerical parameters used to solve these examples are those presented in [10].

3.1.1 Cantilever beam with a uniformly distributed load

This example is a cantilever beam with a uniform load applied on the top surface, as is shown in Figure 1. In this example, the shear-locking effect is present, so it is expected that a precise solution will not be obtained using linear interpolation. In this case it is used $E = 30000$, $\nu = 0.3$,

$L_x = 50$, $L_y = 2$ and $q = 0.1$. In [18] it is possible to find an approximate analytical solution for the stress and displacement field which is more accurate when $L_x \gg L_y$. The displacement at the free end and the stress at $(L_x/2, L_y/4)$ are

$$u_y(L_x, 0) = -\frac{3}{24}\frac{q\,L_x^4}{E\,I},\ \sigma_x(L_x/2, L_y/4) = \frac{1}{960}\left(7\,L_y^2 + 30\,L_x^2\right)\frac{q\,L_y}{I}\,, \tag{8}$$

where $I = L_y^3/12$ is the inertia.

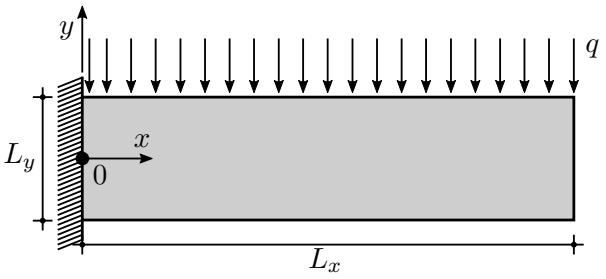

Figure 1: Geometry of the cantilever beam with a uniformly distributed load.

The solution of $u_y(L_x, 0)$ using LRE and MLS methods is shown in Table 1. For linear interpolation, it is possible to see that the exact value is not achieved in all cases as expected due to the shear-locking effect. Nevertheless, with p_1 and LRE, the solution obtained has an error of 0.30%, which is not too large.

Table 1: Solution of $u_y(L_x, 0)$ using LRE and MLS where the analytical solution is $u_y(L_x, 0) = -3.9063$.

LRE							
# Elems	Cardiff [9]	p_1	p_2	p_3	p_4	FF p_1	FF p_2
206	-3.1697	-5.1113	-3.9604	-3.9154	-3.9149	-2.3667	-3.9060
1278	-3.7414	-3.9990	-3.9099	-3.9126	-3.9125	-3.5566	-3.9090
3358	-3.8293	-3.9615	-3.9109	-3.9114	-3.9114	-3.7657	-3.9095
7616	-3.8753	-3.9180	-3.9107	-3.9109	-3.9108	-3.8444	-3.9097
MLS							
# Elems	Cardiff [9]	p_1	p_2	p_3	p_4	FF p_1	FF p_2
206	-3.1697	-4.0308	-3.8865	-3.9159	-3.9149	-2.3667	-3.9060
1278	-3.7414	-3.8047	-3.9013	-3.9114	-3.9121	-3.5566	-3.9090
3358	-3.8293	-3.9983	-3.9112	-3.8283	-3.9115	-3.7657	-3.9095
7616	-3.8753	-4.1010	-3.9100	-3.9113	-3.9107	-3.8444	-3.9097

In Table 2 the solution of $\sigma_x(L_x/2, L_y/4)$ using LRE and MLS is presented. In the case of the 2nd-order method [9], it is possible to see the differences between using MLS or LRE to interpolate the derivatives, being the LRE more accurate.

Table 2: Solution of $\sigma_x(L_x/2, Ly/4)$ using LRE and MLS where the analytical solution is $\sigma_x(L_x/2, Ly/4) = 23.45$.

LRE							
# Elems	Cardiff [9]	p_1	p_2	p_3	p_4	FF p_1	FF p_2
206	12.20	32.73	23.47	23.44	23.44	12.65	23.72
1278	22.22	16.90	23.39	23.44	23.45	26.11	23.46
3358	23.66	23.39	23.44	23.45	23.45	23.13	23.45
7616	22.86	23.30	23.44	23.45	23.45	23.83	23.45
MLS							
# Elems	Cardiff [9]	p_1	p_2	p_3	p_4	FF p_1	FF p_2
206	15.97	18.52	22.14	23.44	23.44	12.65	23.72
1278	22.29	20.20	23.38	23.44	23.45	26.11	23.46
3358	23.87	24.03	23.46	23.43	23.45	23.13	23.45
7616	22.35	22.55	23.46	23.44	23.45	23.83	23.45

3.1.2 Infinite plane containing a stress-free elliptical hole

This example is an infinite plane containing a stress-free elliptical hole and the problem is loaded with a uniform stress at infinity, as shown in the left image of Figure 2. This problem is modeled as shown in the right image of Figure 2: left and bottom boundaries have symmetry conditions while on the rest of the surfaces Neumann conditions are imposed. In this case it is used $E = 1$, $\nu = 0.3$, $a = 1$, $b = 2$, $L_x = L_y = 30$ and $\sigma_x^\infty = 1$. In [17] it is possible to find an analytical expression for the stress $\sigma_y(0, b) = \sigma_x^\infty(1 + 2b/a)$.

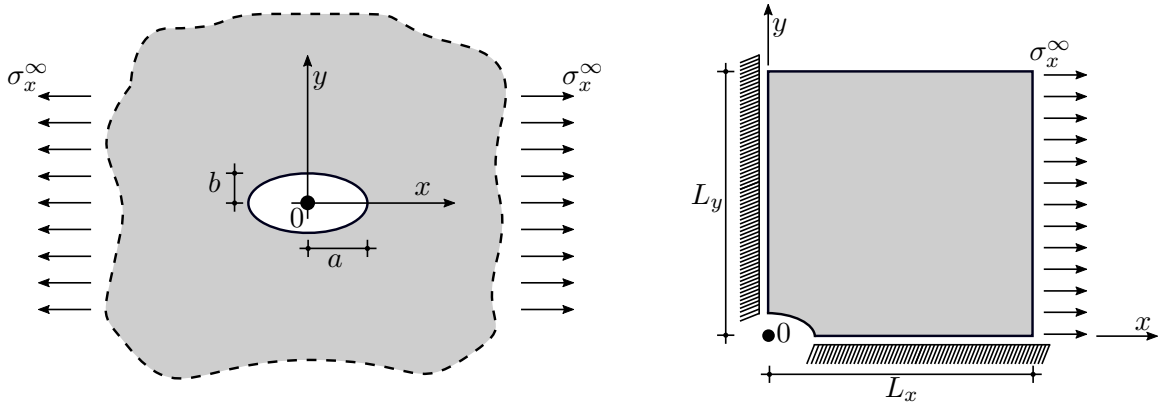

Figure 2: Geometry of the stressed infinite plane with an elliptical hole problem.

In Figure 3 one of the mesh used to solve the problem is presented; it is possible to see that the non unstructured mesh it is needed for this example. In Table 3 the solution of $\sigma_x(0, b)$ using LRE and MLS is presented and it can be seen that both methods work properly.

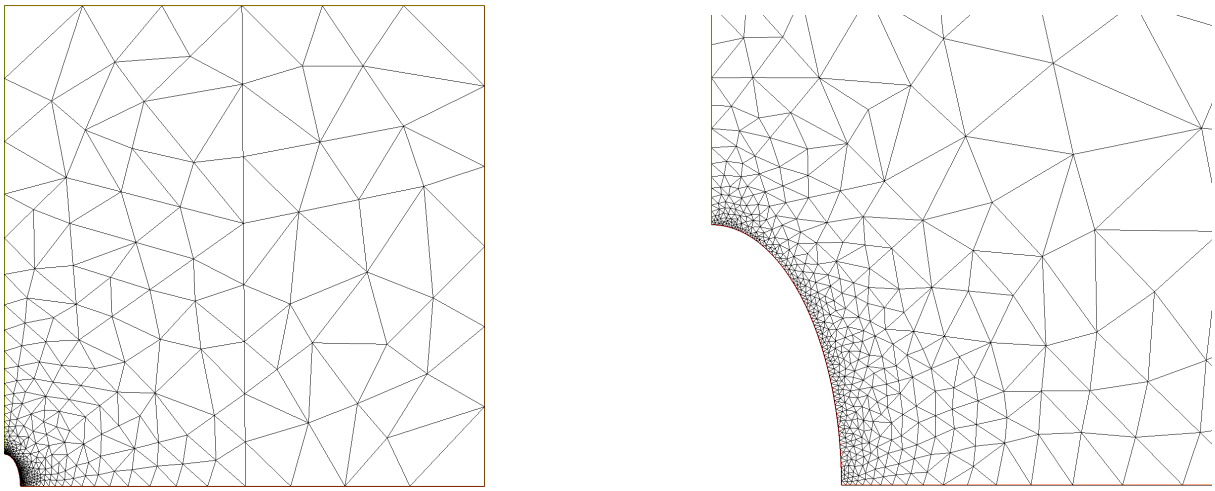

Figure 3: Mesh to solve the infinite plane with an elliptical hole problem.

Table 3: Solution of $\sigma_x(0, b)$ using LRE and MLS where the analytical solution is $\sigma_x(0, b) = 5$.

LRE							
# Elems	Cardiff [9]	p_1	p_2	p_3	p_4	FF p_1	FF p_2
1178	4.921	4.825	5.044	5.062	5.037	4.861	5.041
3454	5.051	4.933	5.092	5.138	5.253	4.974	5.043
6207	5.002	4.953	5.027	5.017	5.004	4.895	5.042
MLS							
# Elems	Cardiff [9]	p_1	p_2	p_3	p_4	FF p_1	FF p_2
1178	4.919	4.770	5.022	5.057	5.479	4.861	5.041
3454	5.040	4.973	5.073	5.125	5.243	4.974	5.043
6207	4.998	4.965	5.022	5.034	5.001	4.895	5.042

3.2 Three-dimensional examples

To solve these examples three interpolations are used: p_1 (linear), p_2 (quadratic) and p_3 (cubic). The high number of points necessary to build the stencil and consequently the high computational cost needed to employ p_4 in 3D cases has influenced the fact of limiting the analysis to p_3. As it was shown in [10], LRE gives much better results than MLS. Additionally, MLS is computationally more expensive because it has to solve a greater number of systems, and this counter-back acquires more importance for the 3D case. Due to these reasons in the first example of Section 3.2.1 only the LRE is used to analyze the parameters of the method for 3D structured meshes. Nevertheless, both methods are used in Section 3.2.2, which is a clamped beam where the shear-locking effect appears.

3.2.1 Analytical example

This example analyzes the error and order of convergence of the LRE and MLS schemes for different parameters of the proposed method in a three-dimensional example using struc-

tured meshes. A known displacement field $\mathbf{u}$ is imposed on the boundary of the domain, and the corresponding volume force $\mathbf{b}$ is imposed in the interior. The domain is a cube $\Omega = (x, y, z) : x, y, z \in [0, 1]$ and the displacement field imposed on the boundary is $\mathbf{u} = u_x\mathbf{e}_x + u_y\mathbf{e}_y + uz\mathbf{e}_z$, where

$$u_x = \log(x + 3)\, y\, (z + 1) + \exp(z),\ u_y = \sin(y\, z) + 3\, y,\ u_z = \exp(x\, z)\, y - 4\, \cos(z). \tag{9}$$

In this example the material properties are $E = 1$ and $\nu = 0.3$. The relative errors in the displacement field $\mathrm{RE}_{\mathbf{u}}$ and in the stress field $\mathrm{RE}_{\boldsymbol{\sigma}}$ are computed in order to observe the influence of the parameters of the method on the results

$$\mathrm{RE}_{\mathbf{u}} = \sqrt{\frac{\int_\Omega \|\mathbf{u} - \mathbf{u}_{\mathrm{num}}\|^2 \mathrm{d}V}{\int_\Omega \|\mathbf{u}\|^2 \mathrm{d}V}}\, 100\% \text{ and } \mathrm{RE}_{\boldsymbol{\sigma}} = \sqrt{\frac{\int_\Omega \|\boldsymbol{\sigma} - \boldsymbol{\sigma}_{\mathrm{num}}\|^2 \mathrm{d}V}{\int_\Omega \|\boldsymbol{\sigma}\|^2 \mathrm{d}V}}\, 100\%\,, \tag{10}$$

and the absolute errors in the displacement field $\mathrm{AE}_{\mathbf{u}}$ and in the stress field $\mathrm{AE}_{\boldsymbol{\sigma}}$ are considered in order to test the convergence order of the method

$$\mathrm{AE}_{\mathbf{u}} = \sqrt{\frac{\int_\Omega \|\mathbf{u} - \mathbf{u}_{\mathrm{num}}\|^2 \mathrm{d}V}{\int_\Omega \mathrm{d}V}} \text{ and } \mathrm{AE}_{\boldsymbol{\sigma}} = \sqrt{\frac{\int_\Omega \|\boldsymbol{\sigma} - \boldsymbol{\sigma}_{\mathrm{num}}\|^2 \mathrm{d}V}{\int_\Omega \mathrm{d}V}}\,. \tag{11}$$

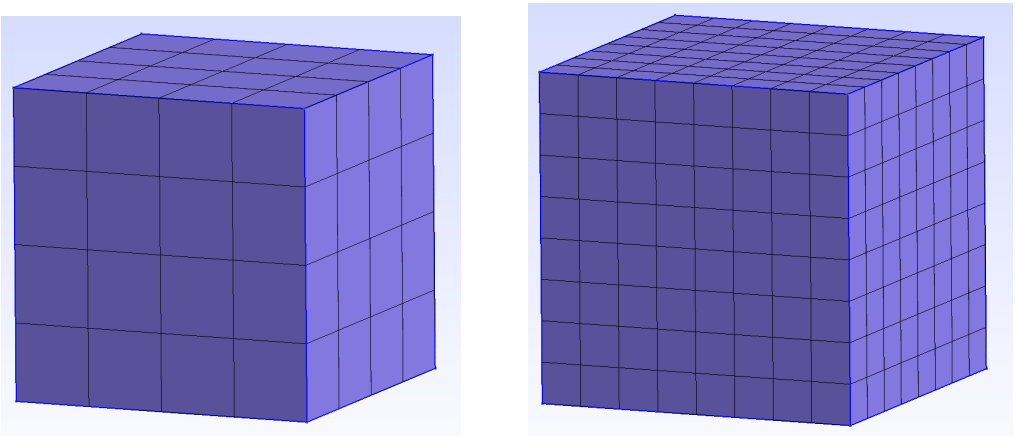

Figure 4: Meshes for the 3D analytical example.

Figure 5 shows a combination of parameters in which the relative error of the displacement field is less than 0.1% for p_2 and p_3 interpolations. The same happens with the stress field, although it can also be seen that the stresses have a more significant error than the displacements, which is expected. From these images, it is possible to conclude that using a parameter $k = 6$ for three-dimensional structured meshes, as in the 2D problem, is an appropriate choice, see [10]. No significant differences are observed when the number of Gauss points varies, but in order to avoid errors in the validation, it is decided to use 49 points in what follows. For the number of stencil points, it is decided to use 14 for p_1, 30 for p_2 and 60 for p_3, which avoids bad conditioning problems obtaining the interpolation coefficients.

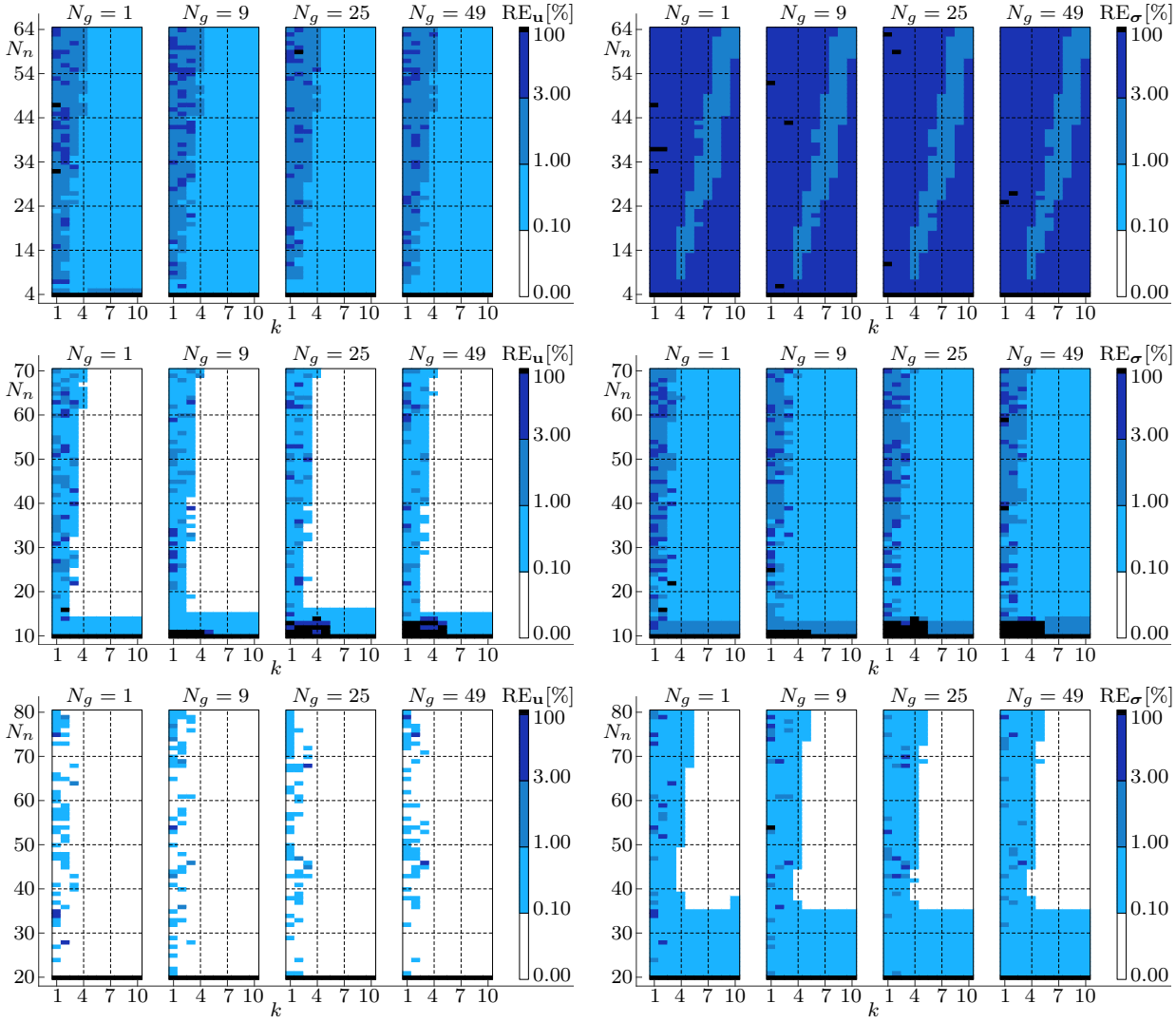

Figure 5: $\mathrm{RE}_{\mathbf{u}}$ [%] (left column) and $\mathrm{RE}_{\boldsymbol{\sigma}}$ [%] (right column) using p_1 (top images), p_2 (middle images) and p_3 (bottom images) for different parameters using LRE method and the mesh shown in the left image of Figure 4.

Figure 6 shows the absolute error obtained for different meshes using the above-mentioned parameters. In this image, it is possible to observe the Order of Convergence (OC) for each interpolation, verifying that the expected order (or higher) is obtained. However, as mentioned in [10], the expected OC for the displacement field using p_2, which is 3, is not adequately obtained. In any case, it is observed that for all cases, the error with p_2 is less than the error using linear interpolation.

3.2.2 Cantilever beam

In this example a three-dimensional cantilever beam subjected to a vertical force at the free end is considered as shown in left image of Figure 7. For this example $E = 30000.0$, $\nu = 0.3$, $L_x = 50$, $L_y = L_z = 2$ and $P = 4$. An analytical solution from [17] is used to compare the

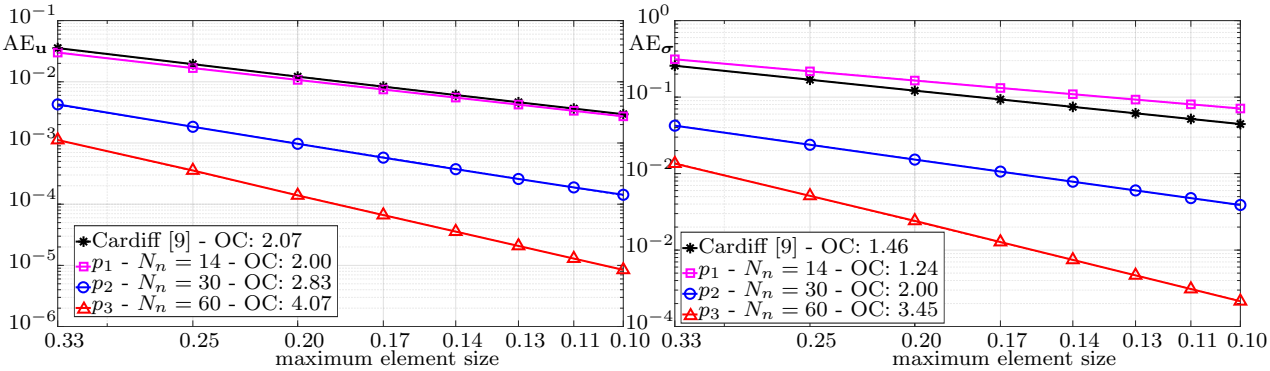

Figure 6: AE$_{\mathbf{u}}$ (left image) and AE$_{\boldsymbol{\sigma}}$ (right image).

numerical results. The right image of Figure 7 shows one of the meshes used to solve this example.

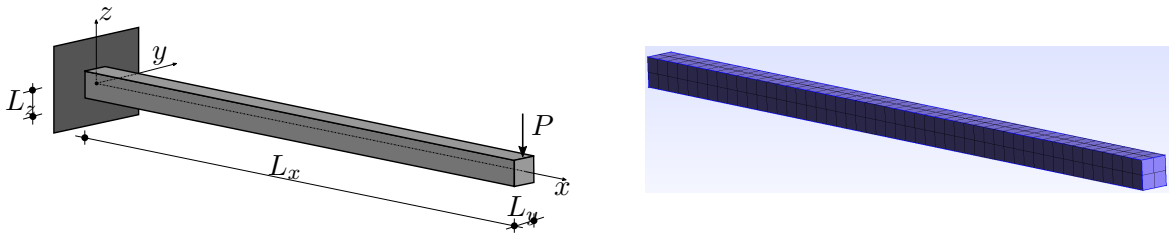

Figure 7: Geometry of three dimension clamped beam.

Tables 4 and 5 show the displacement at the free end and the stress at point $(L_x/2, 0, L_z/4)$, respectively. It can be seen how the results obtained with the LRE are again more accurate than MLS. Results obtained with p_3 are very closed to the analytical solution even for the coarsest meshes, both in terms of displacement and internal stresses. One the other side, in general, p_2 only give good results for the finest mesh, while p_1 shows bad results, being probably strongly affected by the shear locking effect.

Table 4: Solution of $u_z(L_x, 0, 0)$ using LRE and MLS which analytical solution is $u_z(L_x, 0, 0) = -4.1667$.

# Elems	Cardiff [9]	LRE			MLS		
		p_1	p_2	p_3	p_1	p_2	p_3
100	-2.1330	-2.1330	-2.4198	-4.1773	-4.7964	-1.1113	-4.1732
152	-3.1057	-3.1057	-3.9249	-4.1778	-6.8041	-2.1358	-4.1721
200	-3.6570	-3.6570	-4.8549	-4.1786	-6.7136	-3.5345	-4.1719
567	-3.7378	-3.7378	-4.1888	-4.1442	-5.3082	-3.3301	-4.1410

4 CONCLUSIONS

This work presents a high-order interpolation method using the Finite Volume Method to solve the linear elasticity problem. Several examples have been presented in two and three dimensions to validate the method, obtaining acceptable results in all the cases. The high-order

Table 5: Solution of $\sigma_x(L_x/2, 0, L_z/4)$ using LRE and MLS where the analytical solution is $\sigma_x(L_x/2, 0, L_z/4) = 37.50$.

# Elems	LRE				MLS			
	Cardiff [9]	p_1	p_2	p_3	Cardiff [9]	p_1	p_2	p_3
100	17.47	23.26	24.97	37.50	17.50	36.10	10.50	37.50
152	25.83	40.38	34.52	37.50	25.89	-7.92	19.59	37.50
200	30.52	47.79	39.63	37.50	30.60	262.39	32.06	37.50
567	33.43	50.54	37.13	37.32	33.38	63.12	30.22	37.33

interpolation provides accurate results in the examples where the shear locking effect appears. In the extension to a 3D framework of the 2D method presented in [10], it has been shown that there is a suitable combination of parameters that provide accurate results. The LRE method generally shows higher robustness in 3D problems than MLS. Moreover, the computational cost experienced in simulations suggests employing interpolation orders not higher than p_3. The different examples proposed show the capability of the current method to provides accurate results on 2D unstructured and 3D structured meshes subjected to distributed loads. Those fundamental properties are needed to solve the fluid-structure problem of the compressor reed valve, demonstrating the suitability of the method to be included within a three-dimensional software that uses the Finite Volume Method.

ACKNOWLEDGMENTS

P. Castrillo gratefully acknowledges the Universitat Politècnica de Catalunya and Banco Santander for the financial support of his predoctoral grant FPI-UPC (109 FPI-UPC 2018). The authors are supported by the Ministerio de Economía y Competitividad, Spain, RETOtwin project (PDC2021-120970-I00).

REFERENCES

[1] A. Slone, C. Bailey, and M. Cross, "Dynamic solid mechanics using finite volume methods," *Applied Mathematical Modelling*, vol. 27, pp. 69–87, feb 2003.

[2] M. W. Tofique, A. Löf, E. Schillaci, P. Castrillo, and J. Rigola, "Experimental and Numerical Analysis Of Reed Valve Movement In An Impact Fatigue Test System and Reciprocating Compressors," in *International Compressor Engineering Conference*, Purdue University, 2021.

[3] P. Castrillo, E. Schillaci, and J. Rigola, "Simulation of fluid-structure interaction and impact force on a reed valve," in *14th WCCM-ECCOMAS Congress 2020*, vol. 1500, 2021.

[4] L. Cueto-Felgueroso, I. Colominas, X. Nogueira, F. Navarrina, and M. Casteleiro, "Finite volume solvers and Moving Least-Squares approximations for the compressible Navier–Stokes equations on unstructured grids," *Computer Methods in Applied Mechanics and Engineering*, vol. 196, pp. 4712–4736, sep 2007.

[5] S. Khelladi, X. Nogueira, F. Bakir, and I. Colominas, "Toward a higher order unsteady finite volume solver based on reproducing kernel methods," *Computer Methods in Applied Mechanics and Engineering*, vol. 200, pp. 2348–2362, jul 2011.

[6] L. Ramírez, X. Nogueira, S. Khelladi, J.-C. Chassaing, and I. Colominas, "A new higher-order finite volume method based on Moving Least Squares for the resolution of the incompressible Navier–Stokes equations on unstructured grids," *Computer Methods in Applied Mechanics and Engineering*, vol. 278, pp. 883–901, aug 2014.

[7] P. Cardiff and I. Demirdžić, "Thirty years of the finite volume method for solid mechanics," *Archives of Computational Methods in Engineering*, vol. 28, no. 5, pp. 3721–3780, 2021.

[8] I. Demirdžić, "A fourth-order finite volume method for structural analysis," *Applied Mathematical Modelling*, vol. 40, pp. 3104–3114, feb 2016.

[9] P. Cardiff, Ž. Tuković, H. Jasak, and A. Ivanković, "A block-coupled Finite Volume methodology for linear elasticity and unstructured meshes," *Computers & Structures*, vol. 175, pp. 100–122, oct 2016.

[10] P. Castrillo, A. Canelas, E. Schillaci, J. Rigola, and A. Oliva, "High-order finite volume method for linear elasticity on unstructured meshes," *Computers & Structures*, vol. 268, p. 106829, aug 2022.

[11] D. A. Dunavant, "High degree efficient symmetrical Gaussian quadrature rules for the triangle," *International Journal for Numerical Methods in Engineering*, vol. 21, pp. 1129–1148, jun 1985.

[12] L. Shunn and F. Ham, "Symmetric quadrature rules for tetrahedra based on a cubic close-packed lattice arrangement," *Journal of Computational and Applied Mathematics*, vol. 236, pp. 4348–4364, nov 2012.

[13] P. Lancaster and K. Salkauskas, "Surfaces generated by moving least squares methods," *Math. of Computation*, vol. 37, pp. 141–158, jul 1981.

[14] C. Loader, *Local Regression and Likelihood*. Statistics and Computing, New York: Springer-Verlag, 1999.

[15] C. J. Stone, "Consistent Nonparametric Regression," *The Ann. of Stat.*, vol. 5, pp. 5(4):595–620, jul 1977.

[16] F. Hecht, "New development in freefem++," *J. of Numerical Math.*, vol. 20, no. 3-4, pp. 251–265, 2012.

[17] M. H. Sadd, *Elasticity: Theory, Applications, and Numerics*. Elsevier, 2009.

[18] C. xiao Zhan and Y. hua Liu, "Plane elasticity solutions for beams with fixed ends," *Journal of Zhejiang University: Science A*, vol. 16, pp. 805–819, oct 2015.